Available online at www.sciencedirect.com
ScienceDirect
Trans. Nonferrous Met. Soc. China 33(2023) 3364−3375
Transactions of Nonferrous Metals Society of China
www.tnmsc.cn

Design of Ti−7Al−2V alloy with high specific strength by using cluster formula

Zhi-hao ZHU[1], Tian-yu LIU[2], Meng-fan SONG[1], Zhi-peng CHEN[1], Shuang ZHANG[3], Chuang DONG[1,3]

1. Key Laboratory for Materials Modification by Laser, Ion, and Electron Beams of Ministry of Education, School of Materials Science and Engineering, Dalian University of Technology, Dalian 116024, China;
2. State Key Laboratory of Light Alloy Casting Technology for High-end Equipment, Shenyang Research Institute of Foundry Co., Ltd., Shenyang 110022, China;
3. School of Materials Science and Engineering, Dalian Jiaotong University, Dalian 116028, China

Received 26 May 2022; accepted 21 July 2022

Abstract: A near-α Ti−7Al−2V alloy was designed using cluster formula approach and prepared by laser additive manufacturing, whose specific strength is better than that of Ti−6Al−4V alloy. Its composition formula α-$\{[Al-Ti_{12}](AlTi_2)\}_{15}$+$\beta$-$\{[Al-Ti_{14}](V_3)\}_2$ features an enhanced α-Ti by increasing α unit proportion of 15/17 (with respect to 12/17 of Ti−6Al−4V alloy) and stabilized β-Ti via V alloying. This alloy possesses a good laser additive manufacturing processibility. At the as-deposited state, the microstructures are composed of fine basket-weave regions, coarse basket-weave regions and ultrafine α Widmanstätten lath regions. The surface roughness of coarse basket-weave regions is much smaller than that of fine basket-weave regions and ultrafine α Widmanstätten lath regions. The α-phase distribution in fine basket-weave regions is more uniform than that in the coarse basket-weave regions. Its ultimate tensile strength of 971−1005 MPa, yield strength of 891−921 MPa and elongation of 4.5%−6.6% are close to those of Ti−6Al−4V alloy, and particularly, its specific strength of 224−232 kN·m/kg is better than that of Ti−6Al−4V alloy.

Key words: Ti alloy; composition design; cluster-plus-glue-atom model; laser additive manufacturing; mechanical properties

1 Introduction

Laser fabrication has attracted wide attention for the rapid near-net manufacturing of the high-performance components [1−3]. This manufacturing technique is particularly suitable for strategic metallic materials that are difficult and expensive to manufacture through traditional subtractive technologies. Titanium (Ti) alloys are used extensively in the aerospace and biomedical fields due to their excellent performances, including high strength, good biocompatibility, and low density [4,5]. In particular, Ti alloys with good laser additive manufacturing processibilities are key materials for the aerospace industry [6]. Up to now, there are only a few families of special Ti alloys used for laser additive manufacturing, such as α+β-Ti series Ti−6Al−4V [7], TC11 [8], TC21 [9], Ti6246 [10], Ti−Al−Mo−Si−Zr [11], Ti−Al−V−Mo−Nb [12], and β-Ti alloy series Ti−Al−V−Fe [13], Ti−Mo−Zr−Al [14], Ti−Al−Mo [15] and Ti−V−Fe−Al [16]. On the other hand, typical wrought Ti alloys including near-α Ti series Ti1100, IMI834, and Ti60, and β-Ti alloy series β-21S, BT22, Ti-55531, and β-CEZ are not suitable for additive manufacturing because of their wide solidification range, over 100 ℃ in general [17]. As is well known, the solidification rate of the molten metal in the laser additive manufacturing process is 2−3 times

Corresponding author: Chuang DONG, E-mail: dong@dlut.edu.cn
DOI: 10.1016/S1003-6326(23)66339-3

that of conventional casting processes. Ti alloys tend to show severe cracking and poor damage tolerance after laser processing [18,19]. Therefore, there is an urgent need to develop special titanium alloys for laser additive manufacturing.

Ti−6Al−4V alloy has drawn extensive attention due to its excellent additive manufacturing formability, low cost and good workability. Based on the Ti−6Al−4V alloy composition, many Ti−Al−V alloys series have been developed [20,21]. TAN et al [20] investigated the effects of Al and V on laser additive manufactured Ti−(2−11)Al−(4−20)V alloys, and found that the morphology evolution of primary β grains changes from large columnar to small equiaxed as V or Al concentration increases. Among them, near-α alloy series Ti−8Al−2V and Ti−11Al−2V show a better additive-manufacturing formability and a lower density. ZHANG et al [21] developed Ti−(2−11)Al−(1−10)V alloy series based on the neural network model optimization and produced them by laser additive manufacturing. They found that the tensile strengths of Ti−4Al−3V, Ti−5Al−3V, Ti−4Al−4V, and Ti−3Al−6V are comparable to those of wrought Ti−6Al−4V. However, these alloys suffer from insufficient specific strength, below 220 kN·m/kg. The primary issue is then to find high-specific-strength near-α Ti alloys suitable for additive manufacturing, with specific strength above 220 kN·m/kg.

Our team has developed a "cluster-plus-glue-atom" model, a new structural tool for the description of short-range order [22], expressed in the cluster formula as [cluster](glue atoms), which can be understood as the composition gene of the material [23]. With aid of such cluster formula approach, we were able to show the widely-used Ti−6Al−4V composition via a dual-cluster formula to be α-$\{[Al-Ti_{12}](AlTi_2)\}_{12}$+$\beta$-$\{[Al-Ti_{14}](V_2Ti)\}_5$, where the two structural units in proportion of 12:5 correspond respectively to α- and β-Ti phases [7]. This formula provides the basis for the composition optimization of various Ti alloys: by varying the ratio of the α and β units and by alloying the two units separately, different Ti alloys can be formulated, as exemplified in low-elastic-modulus biomedical β-Ti alloys [24], laser additive manufactured α+β Ti alloys [12,25] and high-temperature near-α Ti alloys [17,26]. As far as the objective of the present work is concerned, i.e., achieving high specific strength using additive manufacturing, Ti−Al−V ternary alloys are addressed using the cluster formula approach: the targeted alloy should be near-α type in order to have a low density (henceforth high specific strength) and to ensure a good laser additive manufacturing processibility; it should also contain a certain amount of stable β phase for a good plasticity and high strength.

In the current work, a Ti−7Al−2V alloy was developed based on the dual-cluster formula of Ti−6Al−4V alloy, to address the mentioned limitations. After laser additive manufacturing, this V-lean alloy exhibited a higher specific strength than Ti−6Al−4V alloy.

2 Composition design using cluster formula approach

2.1 Selection of elements

To design a Ti alloy targeting high specific strength with appropriate additive manufacturing processibility, the first step is to ensure a small solidification range. As is known, a wide solidification range tends to induce the formation of microcracks in the alloy [25,27]. In this work, the solidification temperature ranges ($\Delta T_{L\text{-}S}$) of Ti-based binary alloys are estimated using JMatPro software based on Scheil−Gulliver model [12], as given in Fig. 1. In near-α Ti alloys [17], the content of each alloying element does not exceed 25 wt.%. Therefore, the content of alloying element used to calculate the $\Delta T_{L\text{-}S}$ of Ti-based binary alloys is set to be from 0 to 30 wt.%. In the calculation, the starting cooling temperature is set to be 3000 °C, the ending temperature is 25 °C, and the step is 5 °C. When the elemental content contents are less than 15 wt.%, α-Ti stabilizer Al and β-Ti stabilizers Mo, V, Nb, and Ta contribute only weakly to the solidification temperature range: for each 10 wt.% addition, a 5 °C rise of the solidification temperature range is attributed to Al, 6 °C to V, 28 °C to Mo, Nb, and Ta, in sharp contrast to ~150 °C to eutectoid-type β-Ti stabilizers Fe, Cr, and Cu, as shown in Fig. 1. In particular, Al and V are the alloying elements most suitable for laser additive manufacturing.

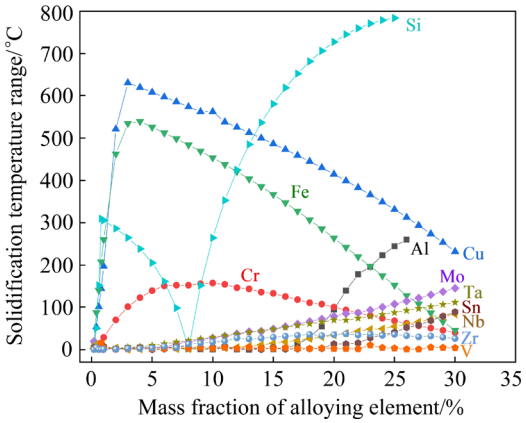

Fig. 1 Solidification temperature ranges of Ti-based binary alloys

2.2 Composition formulas of some Ti alloys for laser additive manufacturing

A quite few Ti alloys such as Ti−6Al−4V [7], TC11 [8], TC21 [9], and Ti6246 [10] have been proved to be suitable for laser additive manufacturing.

The dual-cluster formula of popular Ti−6Al−4V has been well established under a hard-sphere packing model based on the measured phase compositions [7,17]. This alloy is formulated to be α-$\{[Al-Ti_{12}](AlTi_2)\}_{12}$+$\beta$-$\{[Al-Ti_{14}](V_2Ti)\}_5$, consisting of 12 units of HCP α-Ti and 5 units of BCC β-Ti, and the nearest-neighbor clusters of which are respectively twinned cuboctahedron with coordination 12 (Fig. 2(a)) and rhombodo-decahedron with coordination 14 (Fig. 2(b)).

In developing the above formula, each basic α or β unit is treated as a hard sphere whose radius is proportional to the number of atoms in the cluster. It is then assumed that any Ti alloy is formulated to consist of 17 basic α and β units, in different proportions. Typical Ti alloys that are widely accepted for laser additive manufacturing such as TC11, TC21, and Ti6246 are then interpreted using the 17-unit dual-cluster formula, as listed in Table 1. The alloying elements are first classified into the α-Ti stabilizer Al, β-Ti stabilizer $\overline{Mo}$=(Mo, Nb, Cr, Ta, V, Sn, Si, etc.), and solvents $\overline{Ti}$=(Ti, Zr) as already done in Ref. [17]. For example, the nominal composition Ti−6.5Al−3.5Mo−1.5Zr−0.3Si (in wt.%) of TC11, converted to $Ti_{85.81}Al_{11.22}Mo_{1.7}Zr_{0.77}Si_{0.5}$ (in at.%), is simplified into pseudo-ternary $\overline{Ti}_{86.58}$-$Al_{11.22}\overline{Mo}_{2.2}$, where $\overline{Ti}$ =$(Ti_{0.99}Zr_{0.01})$ and $\overline{Mo}$ = $(Mo_{0.77}Si_{0.23})$. The straight line linking the α formula $[Al-\overline{Ti}_{12}]Al\overline{Ti}_2$=$Al_2\overline{Ti}_{14}$ and the alloy composition in the $\overline{Ti}$−Al−$\overline{Mo}$ composition diagram (Fig. 2) passes necessarily the β-Ti one, $[Al-\overline{Ti}_{14}](\overline{Mo}_2\overline{Ti})$= $\overline{Ti}_{15}Al_1\overline{Mo}_2$. Using the lever rule of phase diagram, the numbers of the α and β units are determined and TC11 is finally formulated approximately as α-$\{[Al-Ti_{12}](AlTi_2)\}_{14}$+$\beta$-$\{[Al-Ti_{13.2}Zr_{0.8}](Mo_{1.5}Si_{0.5}Ti)\}_3$, consisting of 14 α-Ti units and 3 β-Ti ones. Similarly, TC21 is formulated as α-$\{[Al-Ti_{12}](AlTi_2)\}_{13}$+ β-$\{[Al-Ti_{13.4}Zr_{0.6}](Sn_{0.57}Mo_{0.71}Nb_{0.74}Cr_{0.98})\}_4$, and Ti6246 as α-$\{[Al-Ti_{12}](AlTi_2)\}_{13}$+$\beta$-$\{[Al-Ti_{12.74}$-$Zr_{1.26}](Mo_{2.36}Sn_{0.64})\}_4$.

All these Ti alloys show dual-cluster formulas maintaining one Al in the β-Ti units. In comparison with popular Ti−6Al−4V, they are characterized by fewer β units (n=3−4) but containing more β stabilizers, such as three β stabilizers in TC21 and three β stabilizers in Ti6246, relative to two β stabilizers in Ti−6Al−4V. In all, there is a paradox that reducing the number of β units can increase laser additive manufacturing processibility, but a certain number of β units are needed to increase the strength and plasticity. To address the above limitations, it can be achieved by optimal matching the number of β unit and enhancing the stability of β unit.

2.3 Alloy design

The next step is to define a suitable composition formula. Two modifications were made in the 17-unit dual-cluster formula α-$\{[Al-Ti_{12}](AlTi_2)\}_{12}$+$\beta$-$\{[Al-Ti_{14}](V_2Ti)\}_5$ of popular Ti−6Al−4V. First, the α unit number is increased from 12 to 15 to enhance laser additive manufacturing processibility and reduce density. Second, the initial β unit $[Al-Ti_{14}]V_2Ti$ of Ti−6Al−4V is transformed to $[Al-Ti_{14}](V_3)$ via more V alloying to improve the β structural stability and the maximum β stability corresponds to the full occupation of the three glue sites. The presence of β unit would also contribute to a good plasticity and high strength comparable to that of Ti−6Al−4V. The designed composition formula then becomes α-$\{[Al-Ti_{12}](AlTi_2)\}_{15}$+$\beta$-$\{[Al-Ti_{14}](V_3)\}_2$, or about Ti−7Al−2V (in wt.%), abbreviated as Ti72 hereafter. It is noted that the chemical composition of Ti72 is close to the conventional laser additive manufactured Ti alloys in $\overline{Ti}$−Al−$\overline{Mo}$ pseudo ternary composition diagram, as shown in Fig. 2. Their Mo and Al equivalents and the dual-cluster composition formulas are listed in Table 1. Ti72

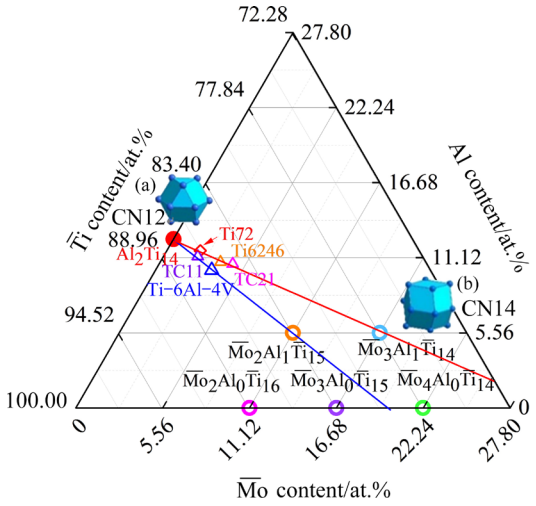

Fig. 2 $\overline{\text{Ti}}$−Al−$\overline{\text{Mo}}$ pseudo-ternary composition diagram showing positions of designed composition (red open square), extending along a straight red line linking α-Al_2Ti_{14} formula and β-$\overline{Mo}_3Al_1\overline{Ti}_{14}$ formula (Nearest-neighbor clusters of the α- and β-Ti, twinned cuboctahedron (a) and rhombic dodecahedron (b) are also shown)

shows a low Mo equivalent and a high Al equivalent, which are respectively 1.3 and 7.0, with reference to those laser of Ti−6Al−4V (2.7 and 6.0), TC11 (3.5 and 6.8), TC21 (5.9 and 7.0), and Ti6246 (6.0 and 7.3). Its solidification temperature range of 6 ℃ as estimated from JMatPro is much smaller than 56 ℃ of TC11, 96 ℃ of TC21 and 51 ℃ of Ti6246, even slightly smaller than 13 ℃ of Ti−6Al−4V, which is indicative of a good additive manufacturing formability comparable to that of Ti−6Al−4V. The Mo equivalent is expressed as [Mo]eq=1.0Mo+1/3.6Nb+1/4.5Ta+1/2W+1/0.63Cr+1/0.65Mn+1/1.5V+1/0.35Fe+1/0.8Ni (in wt.%) [17]. The Al equivalent is expressed as $[Al]_{eq}$=1.0Al+1/3Sn+ 1/6Zr+10O (in wt.%) [28].

3 Experimental

Pure elemental powders, with sizes of 50−150 μm for Ti and 50−75 μm for Al and V, were mixed in a blending machine at ambient temperature. Then, the mixed powders were subjected to laser additive manufacturing under an argon atmosphere using a 6 kW fiber laser (YLS−6000), supplied by IPG Photonics Corporation, Germany. The working parameters were as follows: laser power of 1800 W, beam diameter of 3.0 mm, hatching overlap of 30%, scanning speed of 9 mm/s, powder feeding rate of 8 g/min, and z-axis lifted height of 0.6 mm. The substrate was a commercially Ti−6Al−4V plate, supplied by Yongfeng Non-ferrous Metals Technology Co., Ltd., China. The schematic diagram of the laser additive manufacturing experiment system and scanning scheme are presented in Figs. 3(a, b), respectively. Bulk ingots with dimensions of 60 mm × 15 mm × 30 mm was layer-by-layer deposited using the above parameters, as shown in Fig. 4.

The as-deposited state, without any heat treatment, was characterized for microstructures and properties.

Microstructure characterization of Ti72 alloy was investigated by optical microscopy (OM), scanning electron microscopy (SEM) equipped with an energy dispersive spectrometry (EDS), and X-ray diffraction (XRD). The OM and SEM samples were produced by grinding (using emery papers up to 2000#), polishing (using a SiO_2−H_2O_2 solution), and chemical etching in a 3 vol.% HF+7 vol.% HNO_3+90 vol.% H_2O liquid mixture. The grain sizes of primary β grains, α- and β-phases and

Table 1 Cluster formulas and compositions of designed Ti72 and conventional laser additive manufactured Ti alloys of Ti−6Al−4V, TC11, TC21 and Ti6246

Material	Cluster formula/at.%	Composition/wt.%	$[Mo]^a_{eq}$/wt.%	$[Al]^b_{eq}$/wt.%	$\Delta T^c_{L\text{-}S}$/℃
Ti72	α-$\{[Al-Ti_{12}](AlTi_2)\}_{15}$+$\beta$-$\{[Al-Ti_4](V_3)\}_2$	Ti−7Al−2V	1.3	7.0	6
Ti−6Al−4V	α-$\{[Al-Ti_{12}](AlTi_2)\}_{12}$+$\beta$-$\{[Al-Ti_{14}](V_2Ti)\}_5$	Ti−6Al−4V	2.7	6.0	13
TC11	α-$\{[Al-Ti_{12}](AlTi_2)\}_{14}$+ β-$\{[Al-Ti_{13.2}Zr_{0.8}]\ (Mo_{1.5}Si_{0.5}Ti)\}_3$	Ti−6.5Al−3.5Mo−1.5Zr−0.3Si	3.5	6.8	56
TC21	α-$\{[Al-Ti_{12}](AlTi_2)\}_{13}$+ β-$\{[Al-Ti_{13.4}Zr_{0.6}](Sn_{0.57}Mo_{0.71}Nb_{0.74}Cr_{0.98})\}_4$	Ti−6Al−2Zr−2Sn−3Mo−1.5Cr−2Nb	5.9	7.0	96
Ti6246	α-$\{[Al\text{-}Ti_{12}](AlTi_2)\}_{13}$+ β-$\{[Al-(Ti_{12.74}Zr_{1.26})](Mo_{2.36}Sn_{0.64})\}_4$	Ti−6Al−2Sn−4Zr−6Mo	6.0	7.3	51

[a] $[Mo]_{eq}$=1.0Mo+1/3.6Nb+1/4.5Ta+1/2W+1/0.63Cr+1/0.65Mn+1/1.5V+1/0.35Fe+1/0.8Ni (wt.%) [17]; [b] $[Al]_{eq}$=1.0Al+1/3Sn+1/6Zr+10O (wt.%) [28]; [c] $\Delta T_{L\text{-}S}$ denotes the solidification range of liquid-solid region

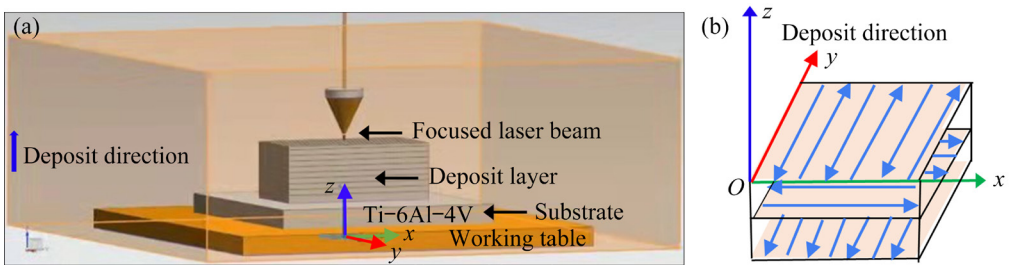

Fig. 3 Schematic diagram of laser additive manufacturing system (a) and laser scanning strategy (b)

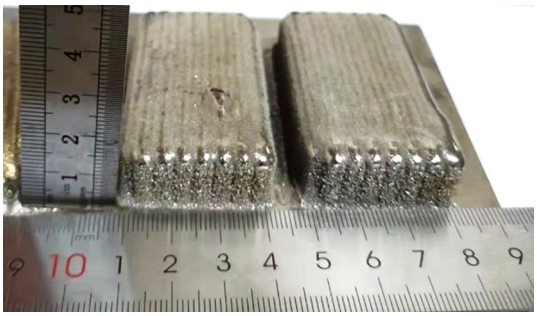

Fig. 4 Macrographs of as-deposited bulk Ti72 samples

their volumetric fractions were calculated by using an Image-Pro Plus 6.0 software. The surface roughness of the samples was investigated by using an Image J software.

Four plate-shaped specimens, machined along the x direction (i.e., within the transverse cross-section) with gage length of 20 mm and a cross-sectional area of 3.5 mm × 2 mm, were subjected to uniaxial tensile tests at room temperature and a strain rate of 0.25 mm/min in a UTM5504−G test machine.

4 Results

4.1 Microstructures of as-deposited state

Figure 5 shows typical growth morphology of laser additive manufactured Ti72 parallel to the deposit z-direction. The microstructure consists of coarse primary β columnar grains with longitudinal lengths of about 650 μm along the deposit direction, which is typical for Ti alloys fabricated by laser additive manufacturing [29]. Besides, layer bands of about 540 μm appear. The formation of coarse columnar β grains is related to the grain growth preferentially along the direction of the fastest heat dissipation (deposit z-direction). The formation of layer bands is caused by the re-melting and re-solidification of the material during the building of the part. From XRD patterns in Fig. 6, it can be seen that the laser additive manufactured Ti72 is composed of α and β phases.

Figure 7 shows optical micrographs of as-deposited Ti72 sample on the transverse cross-section within the layer bands. As shown in Fig. 7(a), this alloy exhibits a mixed structure consisting of ultrafine α Widmanstätten lath regions (marked by red-dotted Area A), fine α phase regions (marked by blue-dotted Area B) and coarser α phase regions (marked by orange-dotted Area C); within the bands there exists a typical basket-weave

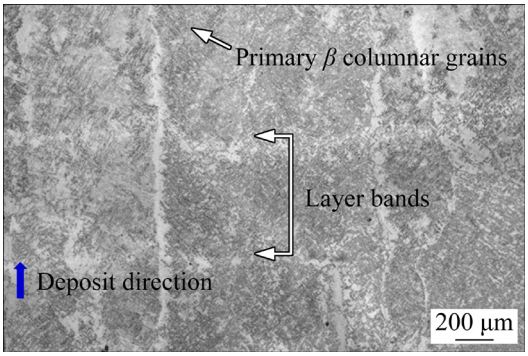

Fig. 5 Typical optical microstructure of as-deposited Ti72 parallel to deposit z-direction

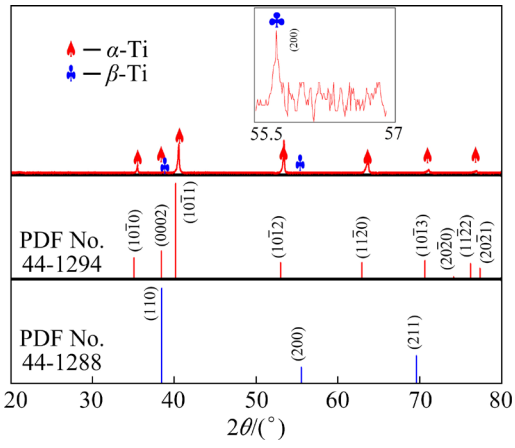

Fig. 6 XRD patterns of as-deposited Ti72 alloy

microstructure composed of lamellar α and remnant β. As marked by the red-dotted Area A in Fig. 7(b), some oriented α Widmanstätten laths are preferentially distributed along the primary β grain boundaries. Similar Widmanstätten microstructure, consisting of oriented lamellar α and remnant β with clear grain boundaries, is also reported in a Ti−6Al−4V [30] and in a laser additive manufactured TC11 [8].

Figure 8 shows secondary electron images taken within the layer bands on the transverse cross-sections of Ti72. It can be seen from the SEM images that two morphologies of the phases appear in Ti72 containing gray lamellar α phases and white strip-like remnant β phases. The volume fraction of β phases in the fine basket-weave regions in Fig. 8(b) is about 7%, noticeably higher than that (5%) of coarse basket-weave regions in Fig. 8(c). Figure 8(d) presents a magnified orange-dotted area of Fig. 8(c). As shown in Fig. 8(d), the phases in the laser additive manufactured Ti72 were analyzed by EDS (Fig. 8(d)), and their components are listed in

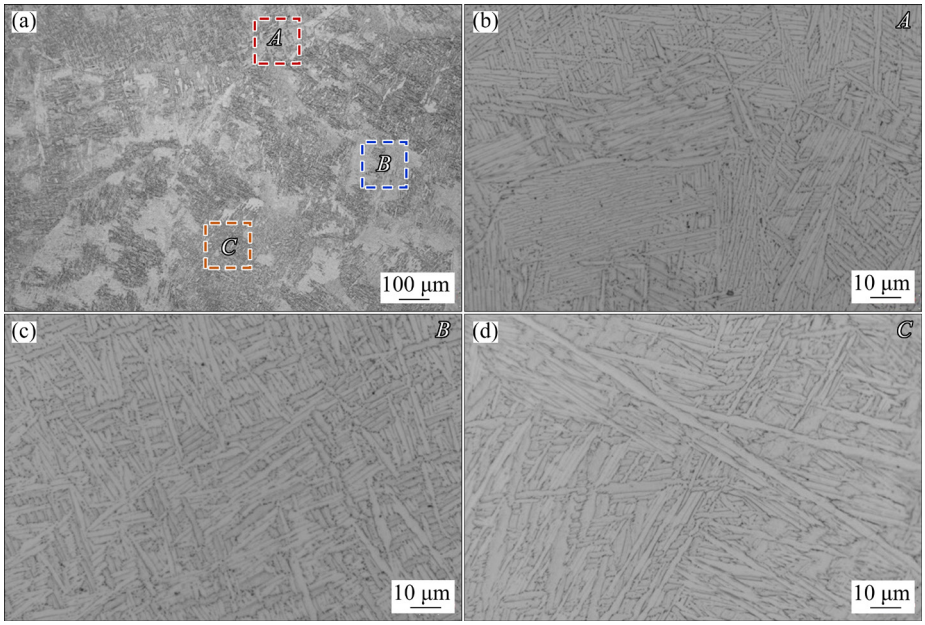

Fig. 7 OM images within layer bands on transverse cross-sections of Ti72 (a), Widmanstätten morphologies taken from red-dotted Area A (b), fine α phase taken from blue-dotted Area B (c), and coarse α phase taken from orange-dotted Area C (d) in (a)

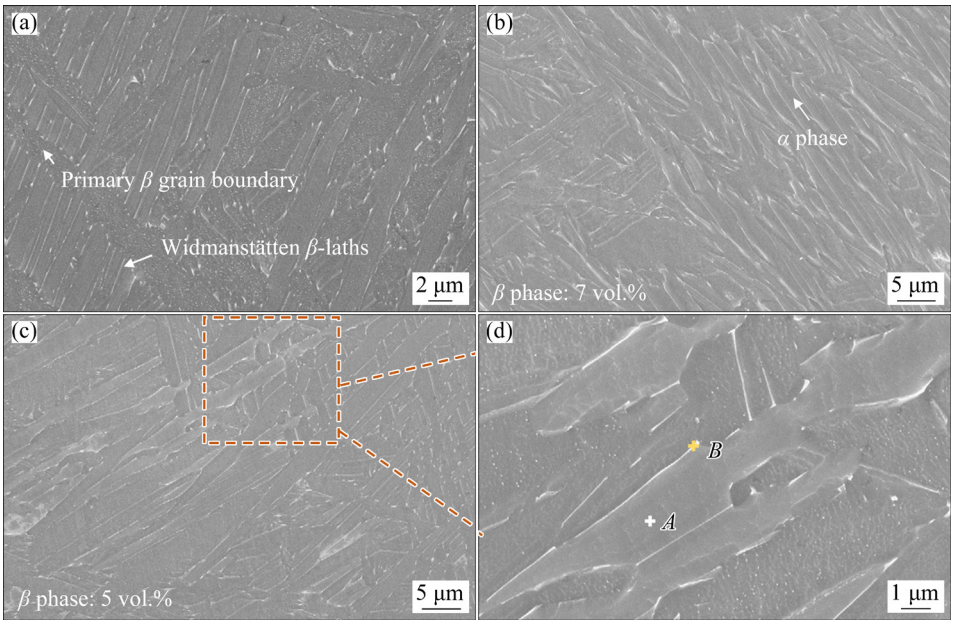

Fig. 8 Secondary electron images taken within layer bands on transverse cross-sections of Ti72: (a) Widmanstätten morphologies; (b) Fine α phase; (c) Coarse α phase; (d) Corresponding EDS points in (c)

Table 2. The results show that the Al/V molar ratio of lamellar α phase (Point A in Fig. 8(d)) is 5.6, while that in white strip-like β phase (Point B in Fig. 8(d)) is 3.9. This suggests that the α phase contains a higher Al concentration and the β phase contains a higher V concentration, confirming the results reported by AZARNIYA et al [30].

Figures 9(a−c) show surface roughness of different regions taken from SEM images of Figs. 8(a−c), respectively. It is evident from Fig. 8 that the surface roughness of Widmanstätten regions (Fig. 9(a)) is about 175 nm and that in fine basket-weave regions (Fig. 9(b)) is about 178 nm, both of which are noticeably higher than that (about 126 nm) of coarse basket-weave regions in Fig. 9(c).

Figures 10(a−c) show α phase size distributions

Table 2 EDS data of α and β phases in Fig. 8(d)

Point	Element content/at.%			Al/V molar ratio
	Ti	Al	V	
A	85.87	12.0	2.13	5.6
B	86.38	10.86	2.76	3.9

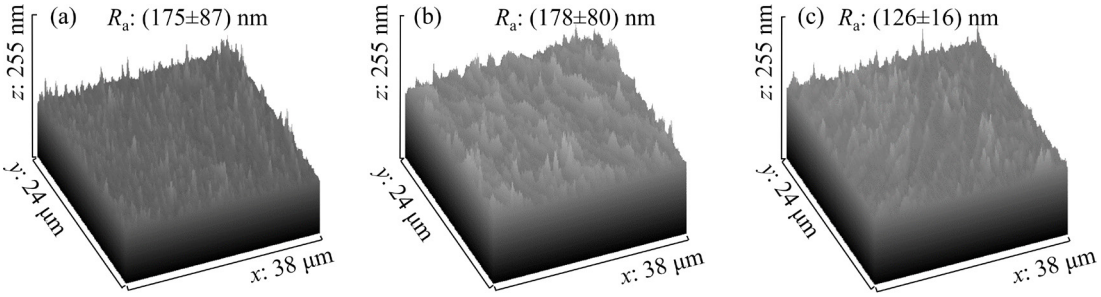

Fig. 9 Surface roughness of Ti72 in different regions taken from SEM images of Fig. 8: (a) Widmanstätten morphology area taken from Area A in Fig. 8(a); (b) Fine α phase area taken from Area B in Fig. 8(b); (c) Coarse α phase area taken from Area C in Fig. 8(c)

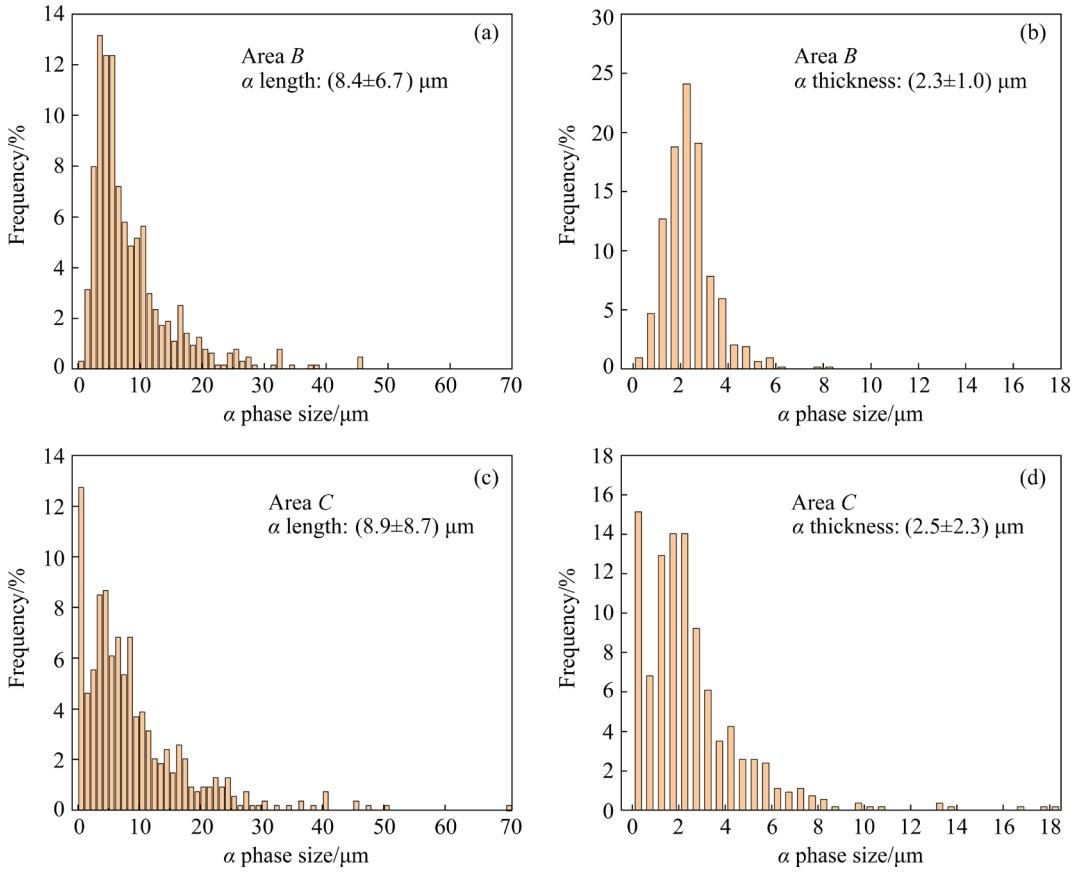

Fig. 10 Size distributions of fine α phase in Ti72 taken from blue-dotted Area B (a, b) and coarse α phase in Ti72 taken from orange-dotted Area C (c, d) in Figs. 7(c) and (d), respectively

in different basket-weave regions taken from Fig. 7(a). The α phase size distribution can be expressed by standard deviation ($SD=\sqrt{\frac{1}{N}\sum_{i=1}^{N}(x_i-r)^2}$), where N is the number of collected α plates, x and r are respectively the single α plate size and an average of α plate size [31]. As shown in Figs. 10(a) and (b), the length and thickness distributions of α plates in Area *B* exhibit a single peak, while those in Area *C* exhibits bimodal structure (Figs. 10(c) and (d)). Statistics results show that the average length and thickness of finer α phases in Area *B* (Fig. 7(c)) are respectively 8.4 and 2.3 μm, in contrast to 8.9 and 2.2 μm in Area *C* (Fig. 7(d)). Moreover, the SD values of α length and thickness in Area *B* are remarkably decreased, about 6.7 and 1.0 μm, respectively, in comparison to about 8.7 and about 2.3 μm in Area *C*. The lower SD value indicates a more uniform α plate distribution.

4.2 Tensile properties

Figure 11 shows the engineering tensile strain−stress curves of Ti72 at ambient temperature. The ultimate tensile strength (UTS), yield strength (YS) and elongation to failure (EL) are listed in Table 3. Ti72 exhibits a good balanced tensile property, UTS of 971−1050 MPa, YS of 887−921 MP, and elongation of 4.5%−6.6%, comparable to those of the reported Ti−6Al−4V [17,32]. As can be seen from Fig. 11, there is a relatively large difference in elongation in the engineering tensile stress−stain curves. This is due to a strong internal stress induced by the high cooling rate of the laser processing, resulting in a larger elongation error. On the other hand, the as-deposited Ti72 alloy without any heat treatment possesses a mixed microstructure containing fine basket-weave regions, coarse basket-weave regions and ultrafine α Widmanstätten lath regions, as shown in Figs. 7 and 8, and also gives rise to a large difference in elongation.

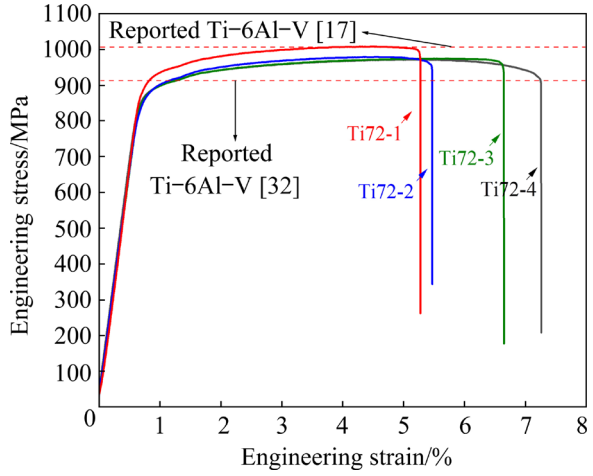

Fig. 11 Engineering tensile stress−stain curves of Ti72 (The red dotted lines respectively donate the reported UTS of Ti−6Al−4V alloys [17,32])

Figure 12 presents comparisons of mechanical properties between Ti72 and the reported conventional additive manufactured Ti alloys. Five density measurements were measured for the Ti72 and the reported Ti−6Al−4V alloy, and the average density was presented in Fig. 12(a). It is noted from Fig. 12(b) that the UTS and EL of Ti72 are in a comparable level with a laser freeform fabricated Ti−6Al−4V alloy [32], particularly its UTS is even better than that of some laser additive manufactured Ti−(2−5)Al−(1−6)V series [21] and a laser additive manufactured TC21 alloy [9] and a wire arc additive manufactured TC11 alloy [33]. YANG et al [34] reported that the yielding-to- tensile ratio (YS/UTS) reflects the strain capacity (i.e., damage tolerance) of the material. A high damage tolerance of metals is generally reflected by YS/UTS close to 0.9 [35], which is also satisfied by Ti72 and most of as-deposited Ti alloys, as shown in Fig. 12(b). In addition, Ti72 exhibits a high specific strength (UTS-to-density) of 224−232 kN·m/kg, increased by 4%−40% with respect to 166−215 kN·m/kg of some reported laser-additive-manufactured Ti−3Al−6V and Ti−(2−5)Al−(1−4)V series [21], and increased by 30% relative to 207 kN·m/kg of a reported laser additive manufactured TC21 alloy [9], superior to 211−230 kN·m/kg of the reported laser additive manufactured Ti−6Al−4V alloys [17,32], even comparable to 234 kN·m/kg of a laser additive manufactured TC11 [8] and 235 kN·m/kg of a direct laser fabricated Ti−6Al−4V [17], as shown in Fig. 12(c). Though the specific strength of Ti72 is lower with reference to those of the laser additive manufactured Ti−5Al−6V [21], Ti−7Al−5V [21], TC17 [36] series and a laser powder bed fusional Ti6246 [10], its density is quite low, about 4.33 g/cm^3, decreased by 5.3% in sharp to the TC17 and Ti6246, over 4.56 g/cm^3.

Table 3 Tensile properties of as-deposited Ti72 (Data from literature are also provided for comparison)

Material	Fabrication method	Tensile property			YS/UTS	Specific strength/ ($kN·m·kg^{-1}$)	Source
		UTS/MPa	YS/MPa	EL/%			
Ti72-1	LAM	1005	921	4.5	0.92	232	This work
Ti72-2	LAM	980	887	4.7	0.91	226	This work
Ti72-3	LAM	973	890	5.9	0.92	225	This work
Ti72-4	LAM	971	891	6.6	0.92	224	This work
Ti−6Al−4V	LAM	1005±20	942±21	10.1±0.6	0.94	230	[17]
Ti−6Al−4V	LAM	965±15	890±30	8±2	0.92	221	[32]
Ti−6Al−4V	LF	911±10	892±10	6.4±0.6	0.98	208	[32]
Ti−6Al−4V	DLD	1025±10	950±2	12±1	0.91	235	[17]
Ti−2Al−1V	LAM	740	665	18	0.90	166	[21]
Ti−4Al−2V	LAM	840	770	15	0.92	190	[21]
Ti−3Al−2V	LAM	840	780	18	0.93	189	[21]
Ti−4Al−3V	LAM	930	845	14	0.91	210	[21]
Ti−5Al−3V	LAM	940	885	9	0.94	214	[21]
Ti−4Al−4V	LAM	900	830	13.5	0.92	203	[21]
Ti−3Al−6V	LAM	965	885	13.5	0.92	215	[21]
Ti−5Al−6V	LAM	1100	1030	7.3	0.94	249	[21]
Ti−7Al−5V	LAM	1150	1070	8.5	0.93	264	[21]
TC11	LAM	1033±13	975±6	6.8±0.2	0.94	234	[8]
TC11	LMD	1018	932	14.7	0.92	231	[37]
TC11	WAAM	935±20	844±16	17.2±2	0.90	212	[33]
TC21	LAM	933	845	16	0.91	207	[9]
TC17	LAM	1201±8	1164±17	5.2±0.7	0.96	262	[36]
TC17	LAM	1138±13	1093±11	11.4±1.0	0.96	248	[36]
Ti6246	LPBF	1183±7	483±6	26.9±0.8	0.41	259	[10]
Ti6246	LPBF	1209±11	582±6	25.5±0.9	0.48	265	[10]

LAM, LF, DLD, LMD, WAAM and LPBF denote laser additive manufacturing, laser freeform fabrication, direct laser fabrication, laser melting deposition, wire arc additive manufacturing and laser powder bed fusion, respectively

5 Conclusions

(1) A near-α Ti72 (Ti−7Al−2V, in wt.%) alloy is designed following the composition formula of α-$\{[Al-Ti_{12}](AlTi_2)\}_{15}$+$\beta$-$\{[Al-Ti_{14}](V_3)\}_2$, which features enhanced α unit proportion of 15/17 (with respect to 12/17 of Ti−6Al−4V) and stabilized β-Ti via V alloying. The Ti72 shows a good laser additive manufacturing processibility, comparable to that of Ti−6Al−4V.

(2) The microstructures of as-deposited Ti72 alloy are composed of fine basket-weave regions, coarse basket-weave regions and ultrafine α Widmanstätten lath regions. The surface roughness of coarse basket-weave regions is much smaller than those of fine basket-weave regions and ultrafine α Widmanstätten lath regions. The α phase distribution in fine basket-weave regions is more uniform than that in the coarse basket-weave regions.

(3) At the as-deposited state, its ultimate tensile strength of 971−1050 MPa, yield strength of 887−921 MPa, and elongation of 4.5%−6.6%, fell are close to those of the reference Ti−6Al−4V, particularly its specific strength of 224−232 kN·m/kg is better than those of Ti−6Al−4V.

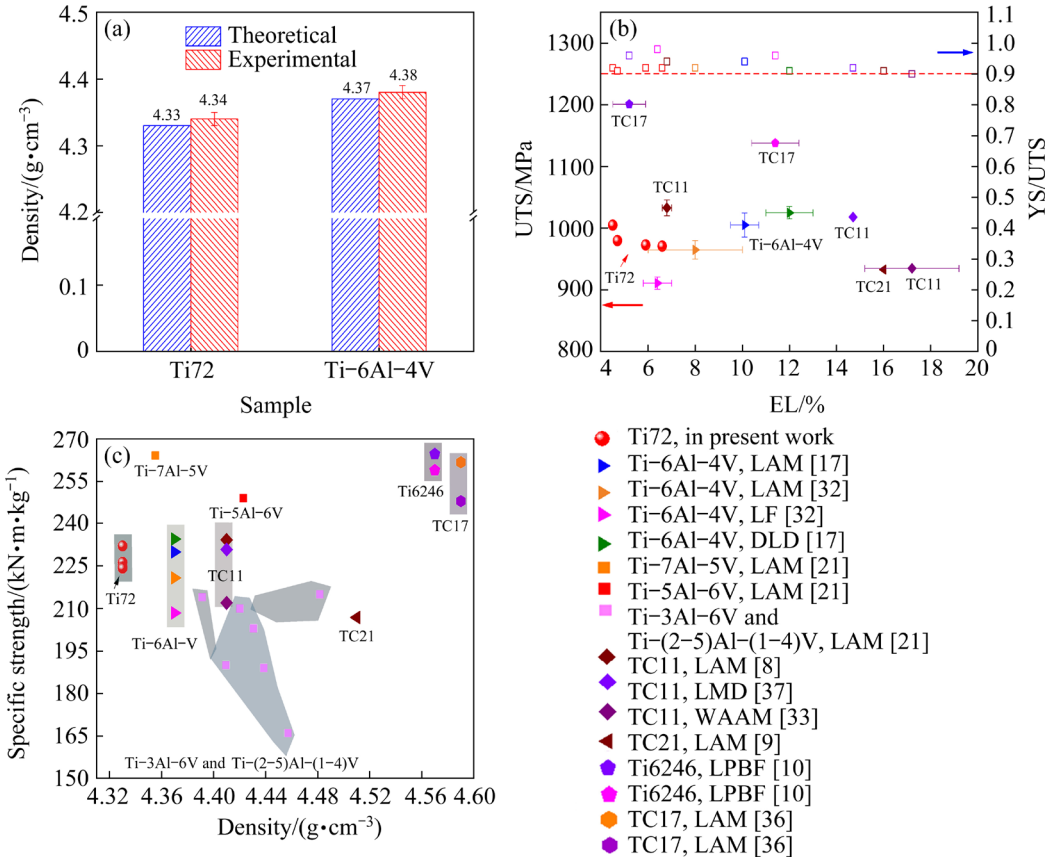

Fig. 12 Comparisons of mechanical properties between Ti72 and reported conventional additive manufactured Ti alloys: (a) Density; (b) Tensile properties; (c) Specific strength

Acknowledgments

This work was financially supported by the Key Discipline and Major Project of Dalian Science and Technology Innovation Foundation, China (No. 2020JJ25CY004), and the National Basic Research Program of China (No. 2020JCJQZD165)

References

[1] YIN Kai, WANG Ling-xiao, DENG Qing-wen, HUANG Qiao-qiao, JIANG Jie, LI Guo-qiang, HE Jun. Femtosecond laser thermal accumulation-triggered micro-/nanostructures with patternable and controllable wettability towards liquid manipulating [J]. Nano-Micro Letters, 2022, 14: 97.

[2] YIN Kai, WU Jun-rui, DENG Qing-wen, WU Zhi-peng, WU Ting-ni, LUO Zhi, JIANG Jie, DUAN Ji-an. Tailoring micro/nanostructured porous polytetrafluoroethylene surfaces for dual-reversible transition of wettability and transmittance [J]. Chemical Engineering Journal, 2022, 434, 134756.

[3] YAN Wen-gao, WANG Hua-ming, TANG Hai-bo, CHENG Xu, ZHU Yan-yan. Effect of Nd addition on microstructure and tensile properties of laser additive manufactured TC11 titanium alloy [J]. Transactions of Nonferrous Metals Society of China, 2022, 32: 1501−1512.

[4] YU Jun, QIN Tuo, LIN Xin, WANG Jun-jie, ZHANG Yu-feng, WANG Shi-yao, YANG Jing-yi, HUANG Wei-dong. Electrochemical dissolution and passivation of laser additive manufactured Ti_6Al_4V controlled by elements segregation and phases distribution [J]. Transactions of Nonferrous Metals Society of China, 2021, 31: 3739−3751.

[5] JU Jiang, LI Jing-jing, JIANG Min, LI Meng-ya, WANG Li-xiang, WANG Kai-ming, YANG Chao, KANG Mao-dong, WANG Jun. Microstructure and electrochemical corrosion behavior of selective laser melted Ti−6Al−4V alloy in simulated artificial saliva [J]. Transactions of Nonferrous Metals Society of China, 2021, 31: 167−177.

[6] REN Hai-shui, TIAN Xiao-jun, LIU Dong, LIU Jian, WANG Hua-ming. Microstructural evolution and mechanical properties of laser melting deposited Ti−6.5Al−3.5Mo−1.5Zr−0.3Si titanium alloy [J]. Transactions of Nonferrous Metals Society of China, 2015, 25: 1856−1864.

[7] LIU Tian-yu, ZHANG Shuang, WANG Qing, MIN Xiao-hua, DONG Chuang. Composition formulas of Ti alloys derived by interpreting Ti−6Al−4V [J]. Science China Technological Sciences, 2021, 64: 1732−1740.

[8] ZHU Yan-yan, LI Jia, TIAN Xiao-jun, WANG Hua-ming, LIU Dong. Microstructure and mechanical properties of hybrid fabricated Ti−6.5Al−3.5Mo−1.5Zr−0.3Si titanium alloy by laser additive manufacturing [J]. Materials Science and Engineering A, 2014, 607: 427−434.

[9] ZHANG Qiang, CHEN Jing, ZHAO Zhuang, TAN Hua, LIN

Xin, HUANG Wei-dong. Microstructure and anisotropic tensile behavior of laser additive manufactured TC21 titanium alloy [J]. Materials Science and Engineering A, 2016, 673: 204−212.

[10] CARROZZA A, AVERSA A, FINO P, LOMBARDI M. A study on the microstructure and mechanical properties of the Ti−6Al−2Sn−4Zr−6Mo alloy produced via laser powder bed fusion [J]. Journal of Alloys and Compounds, 2021, 870: 159329.

[11] JIAO Zong-ge, MA Chen, FU Jun, CHENG Xu, TANG Hai-bo, LIU Dong, ZHANG Ji-kui. The effects of Zr contents on microstructure and properties of laser additive manufactured Ti−6.5Al−3.5Mo−0.3Si−*x*Zr alloys [J]. Journal of Alloys and Compounds, 2018, 745: 592−598.

[12] LIU Tian-yu, ZHU Zhi-hao, ZHANG Shuang, MIN Xiao-hua, DONG Chuang. Design for Ti−Al−V−Mo−Nb alloys for laser additive manufacturing based on a cluster model and on their microstructure and properties [J]. China Foundry, 2021, 18: 424−432.

[13] AZIZI H, ZUROB H, BOSE B, GHIAASIAAN S R, WANG Xiang, COULSON S, DUZ V, PHILLION A B. Additive manufacturing of a novel Ti−Al−V−Fe alloy using selective laser melting [J]. Additive Manufacturing, 2018, 21: 529−535.

[14] SUN Shi-hai, HAGIHARA K, ISHIMOTO T, SUGANUMA R, XUE Yun-fei, NAKANO T. Comparison of microstructure, crystallographic texture, and mechanical properties in Ti−15Mo−5Zr−3Al alloys fabricated via electron and laser beam powder bed fusion technologies [J]. Additive Manufacturing, 2021, 47: 102329.

[15] ZHANG Feng-ying, YANG Meng, CLARE A T, LIN Xin, TAN Hua, CHEN Yong-nan. Microstructure and mechanical properties of Ti−2Al alloyed with Mo formed in laser additive manufacture [J]. Journal of Alloys and Compounds, 2017, 727: 821−831.

[16] JIAO Zong-ge, FU Jun, LI Zhuo, CHENG Xu, TANG Hai-bo, WANG Hua-ming. The spatial distribution of α phase in laser melting deposition additive manufactured Ti−10V−2Fe−3Al alloy [J]. Materials & Design, 2018, 154: 108−116.

[17] ZHU Zhi-hao, LIU Tian-yu, DONG Chuang, DONG Dan-dan, ZHANG Shuang, WANG Qing. Achieving high-temperature strength and plasticity in near-α Ti−7Al−3Zr−2V alloy using cluster formula design [J]. Journal of Materials Research and Technology, 2022, 18: 2582−2592.

[18] MOEINFAR K, KHODABAKHSHI F, KASHANI-BOZORG S F, MOHAMMADI M, GERLICH A P. A review on metallurgical aspects of laser additive manufacturing (LAM): Stainless steels, nickel superalloys, and titanium alloys [J]. Journal of Materials Research and Technology, 2022, 16: 1029−1068.

[19] ZHANG Tian-long, LIU Chain-tsuan. Design of titanium alloys by additive manufacturing: A critical review [J]. Advanced Powder Materials, 2021, 1: 100014.

[20] TAN Hua, ZHANG Feng-ying, CHEN Jing, LIN Xin, HUANG Wei-dong. Microstructure evolution of laser solid forming of Ti−Al−V ternary system alloys from blended elemental powders [J]. Chinese Optics Letters, 2011, 9: 051403.

[21] ZHANG Feng-ying, TAN Hua, CHEN Jing, LIN Xin. Mechanical properties of laser solid formed Ti−Al−V ternary system titanium alloys [J]. Chinses Journal of Lasers, 2012, 39: 1−7. (in Chinese)

[22] DONG Chuang, CHEN Wei-rong, WANG Ying-min, QIANG Jian-bing, WANG Qing, LEI Yi, CALVO-DAHLBORG M, DUBOIS J M. Formation of quasicrystals and metallic glasses in relation to icosahedral clusters [J]. Journal of Non-Crystalline Solids, 2007, 353: 3405−3411.

[23] ZHANG Shuang, WANG Qing, DONG Chuang. Composition genes in materials [J]. Journal of Materials Informatics, 2021, 1: 8.

[24] WANG Qing, JI Chun-jun, WANG Ying-min, QIANG Jian-bing, DONG Chuang. β-Ti alloys with low young's moduli interpreted by cluster-plus-glue-atom model [J]. Metallurgical and Materials Transactions A, 2012, 44: 1872−1879.

[25] LIU Tian-yu, MIN Xiao-hua, ZHANG Shuang, WANG Cun-shan, DONG Chuang. Microstructures and mechanical properties of Ti−Al−V−Nb alloys with cluster formula manufactured by laser additive manufacturing [J]. Transactions of Nonferrous Metals Society of China, 2021, 31: 3012−3023.

[26] CHE Jin-da, JIANG Bei-bei, WANG Qing, ZHANG Rui-qian, TANG Rui, CHEN Guo-qing, DONG Chuang. Effects of minor Hf/Ta/Nb additions on high-temperature oxidation-resistant properties of near α-Ti alloys [J]. The Chinese Journal of Nonferrous Metals, 2016, 26: 2086−2092. (in Chinese)

[27] YU Qun, WANG Cun-shan, WANG Di, MIN Xiao-hua. Microstructure and properties of Ti−Zr congruent alloy fabricated by laser additive manufacturing [J]. Journal of Alloys and Compounds, 2020, 834: 155087.

[28] KITASHIMA T, SURESH K S, YAMABE-MITARAI Y. Effect of germanium and silicon additions on the mechanical properties of a near-α titanium alloy [J]. Materials Science and Engineering A, 2014, 597: 212−218.

[29] FAN Wei, TAN Hua, ZHANG Feng-ying, FENG Zhe, WANG Yong-xia, ZHANG Lai-chang, LIN Xin, HUANG Wei-dong. Overcoming the limitation of in-situ microstructural control in laser additive manufactured Ti−6Al−4V alloy to enhanced mechanical performance by integration of synchronous induction heating [J]. Journal of Materials Science & Technology, 2021, 94: 32−46.

[30] AZARNIYA A, COLERA X G, MIRZAALI M J, SOVIZI S, BARTOLOMEU F, WEGLOWSKI M K S, WITS W W, YAP C Y, AHN J, MIRANDA G, SILVA F S, MADAAH-HOSSEINI H M, RAMAKRISHNA S, ZADPOOR A A. Additive manufacturing of Ti−6Al−4V parts through laser metal deposition (LMD): Process, microstructure, and mechanical properties [J]. Journal of Alloys and Compounds, 2019, 804: 163−191.

[31] ZHU Zhi-hao, NIE Kai-bo, MUNROE P, DENG Kun-kun, GUO Ya-chao, HAN Jun-gang. Synergistic effects of hybrid (SiC+TiC) nanoparticles and dynamic precipitates in the design of a high-strength magnesium matrix nanocomposite [J]. Materials Chemistry and Physics, 2021, 259: 124048.

[32] DEBROY T, WEI H L, ZUBACK J S, MUKHERJEE T, ELMER J W, MILEWSKI J O, BEESE A M, WILSON-HEID A, DE A, ZHANG W. Additive manufacturing of metallic components—Process, structure and properties [J]. Progress in Materials Science, 2018, 92: 112−224.

[33] LI Yang-yang, MA Shu-yuan, LIU Chang-meng, ZHANG Meng. Microstructure and mechanical properties of Ti−6.5Al−3.5Mo−1.5Zr−0.3Si alloy fabricated by arc additive manufacturing with post heat treatment [J]. Key Engineering Materials, 2018, 789: 161−169.

[34] YANG Yue, ZHANG Hong, WU Kai, CHEN Peng-chao, SUI Yong-li, YANG Dai, LIU Xiao-ben. Strain capacity analysis of the mismatched welding joint with misalignments of *D*1422 mm X80 steel pipelines: An experimental and numerical investigation [J]. Journal of Pipeline Science and Engineering, 2021, 1: 212−224.

[35] CAO Yue-jie, CAO Zeng-qiang, ZUO Yang-jie, HUO Lu-bin, QIU Jian-ping, ZUO Du-quan. Numerical and experimental investigation of fitting tolerance effects on damage and failure of CFRP/Ti double-lap single-bolt joints [J]. Aerospace Science and Technology, 2018, 78: 461−470.

[36] ZHU Yan-yan, CHEN Bo, TANG Hai-bo, CHENG Xu, WANG Hua-ming, LI Jia. Influence of heat treatments on microstructure and mechanical properties of laser additive manufacturing Ti−5Al−2Sn−2Zr−4Mo−4Cr titanium alloy [J]. Transactions of Nonferrous Metals Society of China, 2018, 28: 36−46.

[37] ZHU Yan-yan, TIAN Xiang-jun, LI Jia, WANG Hua-ming. The anisotropy of laser melting deposition additive manufacturing Ti−6.5Al−3.5Mo−1.5Zr−0.3Si titanium alloy [J]. Materials & Design, 2015, 67: 538−542.

团簇式方法设计具有高比强度的 Ti−7Al−2V 合金

朱智浩[1]，刘田雨[2]，宋梦凡[1]，陈志鹏[1]，张 爽[3]，董 闯[1,3]

1. 大连理工大学 材料科学与工程学院 三束材料改性教育部重点实验室，大连 116024；
2. 沈阳铸造研究所有限公司 高端装备轻合金铸造技术国家重点实验室，沈阳 110022；
3. 大连交通大学 材料科学与工程学院，大连 116028

摘 要：基于团簇式设计方法，采用激光增材制造工艺制备一种近 α 型 Ti−7Al−2V 合金，其比强度优于 Ti−6Al−4V 合金的比强度。该合金的成分式为 α-{[Al−Ti$_{12}$](AlTi$_2$)}$_{15}$+β-{[Al−Ti$_{14}$](V$_3$)}$_2$：其特征在于 α 结构单元比例提高为 15/17(相对于 Ti−6Al−4V 的 12/17)，使合金成分偏向 α-Ti；通过 V 元素合金化，提高了 β-Ti 结构单元稳定性。该合金具有良好的激光增材制造成形性。沉积态下，该合金的显微组织由细网篮组织区、粗网篮组织区和超细 α 魏氏组织区构成。其中，粗网篮组织区的表面粗糙度明显低于细网篮组织区和超细 α 魏氏组织区的表面粗糙度。细网篮组织区的 α 相分布相比于粗网篮组织区更加均匀。该合金的抗拉强度为 971~1005 MPa，屈服强度为 891~921 MPa，伸长率为 4.5%~6.6%，均与 Ti−6Al−4V 的相近，尤其是该合金的比强度为 224~232 kN·m/kg，优于 Ti−6Al−4V 合金的比强度。

关键词：钛合金；成分设计；团簇加连接原子模型；激光增材制造；力学性能

(Edited by Wei-ping CHEN)